The Pennsylvania State University

The Graduate School

Department of Mechanical and Nuclear Engineering

DESIGN OF CIRCULARLY TOWED CABLE-BODY SYSTEMS

A Thesis in

Mechanical Engineering

by

Siva Sankara Varma Gottimukkala

Submitted in Partial Fulfillment

of the Requirements

for the Degree of

Master of Science

August 2011

The thesis of Siva Sankara Varma Gottimukkala was reviewed and approved* by the following:

Christopher D. Rahn
Professor of Mechanical engineering
Thesis Advisor

Eric Mockensturm
Associate Professor of Mechanical Engineering

Karen A. Thole
Professor of Mechanical Engineering
Head of the Department of Mechanical and Nuclear Engineering

*Signatures are on file in the Graduate School.

Abstract

Circularly towed cable-body systems can be used to pick-up and deliver payloads, provide surveillance, and tow aerial and marine vehicles. To provide a stable operating platform, the body or end mass should have a unique and stable steady state solution with small diameter so that it travels at a much slower speed than the tow vehicle. In this thesis, the minimum damping is calculated that ensures the stable single valued steady state solutions as a function of non-dimensional system parameters including cable length and end mass. Steady state solutions are found using the numerical continuation and bifurcation analysis and Galerkin's method provides the linearized vibration equations that determine stability. Bifurcation analysis is also used to find the minimum achievable end mass radius. A design algorithm is presented and demonstrated using an example.

Table of Contents

List of Figures

List of Tables

Acknowledgments

I wish to acknowledge my advisor Dr. Chris Rahn for his valuable suggestions and encouragement throughout my thesis work. I thank Dr. Eric Mockensturm for kindly reviewing the thesis and giving valuable feedback. I wish to thank my friend and labmate, Deepak Trivedi, for his guidance during the initial phases of the project. I am grateful to my parents who actively supported me during my entire graduate studies without whom my success would be incomplete. I wish to thank the Pennsylvania State University and the department of Mechanical Engineering for providing the computational resources necessary to complete my project. Finally, I would like to thank IATech for providing funding for the project.

Chapter 1

Introduction

Circularly towed cable body systems (CTCBS) have been studied for several decades for their fascinating dynamic behavior and their numerous applications in aerial and marine environments. In these systems, a cable is towed from a tow vehicle moving in a constant circular motion in gravitational field with a mass attached at the bottom end of the cable. For sufficiently high aerodynamic drag and cable length, the attached mass rotates in a small circle and appears almost stationary with respect to the inertial frame. If the systems is stable in this configuration, then the payload can be used for delivery [1] and surveillance [2]. This approach has also been used in marine applications [3] and the autonomous aerial recovery of unmanned aircraft [4].

The steady state solutions of the CTCBS and their dynamic behavior are studied in [1, 5, 6]. Russell and Anderson [1] developed a finite element model to study the steady state solutions and stability of a continuous CTCBS. If the aerodynamic drag is insufficient then the system exhibits jump phenomena and buckling and flutter instabilities for certain rotation speed ranges. Zhu and Rahn [5] obtain the steady state solutions from nonlinear equations of motion and analyze the stability of these solutions using Galerkin's method. Multiple steady state solutions are calculated for low cable drag

and stable single-valued solutions for sufficiently low rotation speed. Limit cycle oscillations of whirling cable and their stability are studied by Clark and Fraser [6]. The whirling cable gain additional loops as the angular velocity increases and instabilities occur at the turning points and Hopf points on the bifurcation curve. Williams and Trivalio [2] obtained optimal cable configurations given the performance limitations on the tow vehicle. A lumped parameter model is used to calculate the achievable end mass radius for different angular velocities and tow-point velocities. Optimal system parameters are determined based on the performance limitations of the towing aircraft.

This thesis extends the work of [2] by focusing on the design of stable CTCBS. A non-dimensional analysis is used to make the results generally applicable to CTCBS, irrespective of the scale and environment. Bifurcation analysis is used to determine the minimum achievable end mass radius. The minimum damping required to prevent flutter and divergence instabilities is determined. A general design procedure is introduced and applied to a Micro Air Vehicle recovery application.

Chapter 2

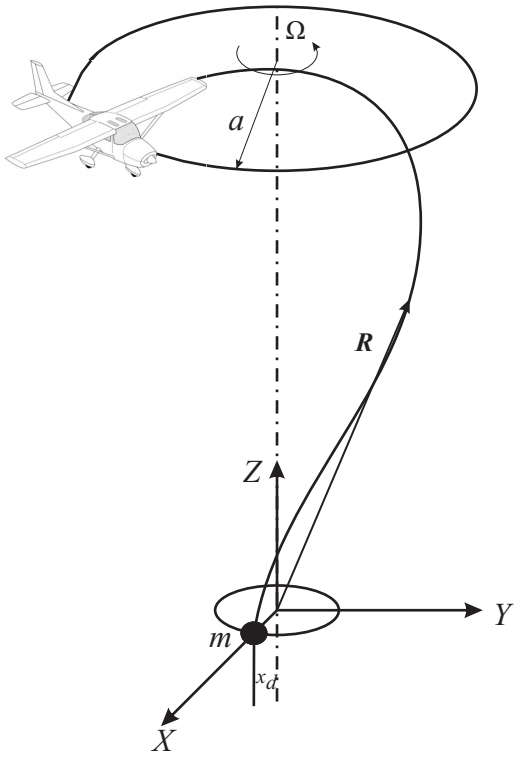

Figure 2.1. Schematic of the circularly towed cable-body system

Mathematical Model

A schematic diagram of a CTCBS is shown in Figure 1. The tow vehicle rotates in a circle of radius a with constant angular velocity Ω about a vertical axis. A cable with end mass M is attached to the tow vehicle. The position of each point along the cable is represented in a rotating reference frame XYZ as a function of the arc length coordinate S. The Z axis is aligned with the rotation axis and the X axis intersects the steady state end mass position. The position vector of any point on the cable is denoted by $\mathbf{R}(S,T)$ where T is the time. Vectors $\mathbf{R}_1$ and $\mathbf{R}_2$ are the steady state and the perturbed configurations, respectively. The displacement relative to the steady state configuration

$$\mathbf{U}(S_0,T) = \mathbf{R}_2 - \mathbf{R}_1, \tag{2.1}$$

where S_0 is the arc length coordinate of the cable in the unstretched configuration. The cable has a cross sectional area A_0 in the unstretched configuration.

2.1 Governing Equations

Tension, gravity and drag forces act on the cable. The equations of motion are derived by applying Newton's law to a small cable element [5]. The cable is assumed to be extensible and the tangential component of the drag is assumed to be negligibly small. The non-dimensional equations of motion [5] are given by

$$\frac{\partial}{\partial s}\left(\frac{p\epsilon_2}{\epsilon_1}\left(\frac{\partial \mathbf{r}}{\partial s}+\frac{\partial \mathbf{u}}{\partial s}\right)\right)$$

$$= \rho\mathbf{k} + \omega^{\mathbf{2}}\left\{\mathbf{k}\times(\mathbf{k}\times\mathbf{r}) + \mathbf{k}\times(\mathbf{k}\times\mathbf{r}) + \mathbf{2k}\times\frac{\partial\mathbf{u}}{\partial\mathbf{t}} + \frac{\partial^{\mathbf{2}}\mathbf{u}}{\partial\mathbf{t^2}}\right\} + \mathbf{d_n}|\mathbf{v_n^f}|\mathbf{v_n^f}, \quad (2.2)$$

where

$$\mathbf{r} = \mathrm{x}\mathbf{i} + \mathrm{y}\mathbf{j} + \mathrm{z}\mathbf{k} = \frac{\mathbf{R_1}}{\mathrm{a}}, \;\; \mathrm{s} = \frac{\mathrm{S}_0}{\mathrm{a}}, \;\; \mathbf{u} = \frac{\mathbf{U}}{\mathrm{a}}, \;\; \mathrm{t} = \Omega\mathrm{T}, \quad (2.3)$$

$$\omega^2 = \frac{a\Omega^2}{g}, \;\; \rho = \frac{\rho_a}{\rho_b}, \;\; d_n = \frac{D_n a}{\rho_a A_0}, \;\; p = \frac{P_1}{\rho_a A_0 a g}, \quad (2.4)$$

$$\gamma = \frac{E}{\rho_a a g}, \;\; \epsilon_1 = \frac{p}{\gamma}, \;\; \epsilon_2 = \epsilon_1 + \frac{\partial\mathbf{r}}{\partial s}\frac{\partial\mathbf{u}}{\partial s} + \frac{1}{2}\frac{\partial\mathbf{u}}{\partial s}\frac{\partial\mathbf{u}}{\partial s}, \quad (2.5)$$

and

$$\mathbf{v}_n^f = \frac{\partial(\mathbf{r}+\mathbf{u})}{\partial s}\times\left(\left(\frac{\partial\mathbf{u}}{\partial t} + \mathbf{k}\times(\mathbf{u}+\mathbf{r})\right)\times\frac{\partial(\mathbf{r}+\mathbf{u})}{\partial s}\right). \quad (2.6)$$

The natural boundary conditions associated with the end mass at $s = 0$ are

$$\begin{aligned}\frac{p_d\epsilon_2}{\epsilon_1}&\left(\frac{\partial\mathbf{r}}{\partial s} + \frac{\partial\mathbf{u}_d}{\partial s}\right)\\ &= w\mathbf{k} + m\omega^2\left\{\mathbf{k}\times(\mathbf{k}\times\mathbf{r}) + \mathbf{k}\times(\mathbf{k}\times\mathbf{u}_d) + 2\mathbf{k}\times\frac{\partial\mathbf{u}_d}{\partial t} + \frac{\partial^2\mathbf{u}_d}{\partial t^2}\right\}\\ &\quad + d\omega^2\left|\frac{\partial\mathbf{u}_d}{\partial t} + \mathbf{k}\times(\mathbf{u}_d+\mathbf{r})\right|\left(\frac{\partial\mathbf{u}_d}{\partial t} + \mathbf{k}\times(\mathbf{u}_d+\mathbf{r})\right), \end{aligned} \quad (2.7)$$

where p_d is the cable tension at $s = 0$ and

$$w = \frac{W}{\rho_a a A_0 g}, \quad m = \frac{M}{\rho_a a A_0}, \quad d = \frac{D}{\rho_a A_0}, \quad \mathbf{u}_d = \frac{\mathbf{U}_d}{a}. \quad (2.8)$$

The geometric boundary conditions for the model are

$$x = \frac{X_d}{a} = x_d, \quad y = z = 0 \;\; at \;\; s = 0, \quad (2.9)$$

$$x^2 + y^2 = 1, \quad \mathbf{u} = 0 \;\; at \;\; s = \frac{L}{a} = l. \quad (2.10)$$

Here, ρ_a and ρ_b are the cable densities including the added mass and buoyancy, respectively; ϵ_1 is the strain at steady state configuration; P_1 is the steady state cable tension and W the weight of the end mass; U_d is the perturbation at $s = 0$; and D_n and D are the drag coefficients of the cable and the end mass.

2.2 Steady State Equations

The steady state or quasi-stationary solutions appear stationary with respect to the rotating coordinate frame. The steady state equations are obtained by substituting $\mathbf{u} = 0$ in the Eq. (2.2). The scalar steady state equations are

$$px_{,ss} = -p_{,s}x_{,s} + \omega^2\{-x - d_n|\mathbf{v}_n^i|y - x_{,s}(yx_{,s} - y_{,s}x)\}, \tag{2.11}$$

$$py_{,ss} = -p_{,s}y_{,s} + \omega^2\{-y + d_n|\mathbf{v}_n^i|x - y_{,s}(xy_{,s} - x_{,s}y)\}, \tag{2.12}$$

$$pz_{,ss} = \rho - p_{,s}z_{,s} + \omega^2 d_n|\mathbf{v}_n^i|z_{,s}(yx_{,s} - y_{,s}x), \tag{2.13}$$

where $(.)_{,s} = d(.)/ds$ and

$$|\mathbf{v}_n^i| = [z_{,s}^2(x^2 + y^2) + (xx_{,s} + yy_{,s})^2]^{1/2}. \tag{2.14}$$

The boundary conditions at $s = 0$ are

$$\frac{dx}{ds} = -\omega^2\frac{mx_d}{p_d}, \quad \frac{dy}{ds} = d\omega^2\frac{x_d^2}{p_d}, \quad \frac{dz}{ds} = \frac{w}{p_d}, \tag{2.15}$$

$$x = x_d, \quad y = z = 0, \tag{2.16}$$

and at $s = l$

$$x(l)^2 + y(l)^2 - 1 = 0. \tag{2.17}$$

The steady state cable tension

$$p = p_d + \rho z + \frac{\omega^2}{2}(x_d^2 - x^2 - y^2). \tag{2.18}$$

2.3 Vibration Equations

The linearized vibration equations [5] are obtained by cancellation of steady state terms from Eq. (2.2) and linearization of $\mathbf{u}(s,t)$ around the steady state to produce the vibration equations

$$\begin{aligned}\frac{\partial}{\partial s}\left[\gamma\left(\frac{\partial \mathbf{r}}{\partial s}.\frac{\partial \mathbf{u}}{\partial s}\right)\frac{\partial \mathbf{r}}{\partial s} + p\frac{\partial \mathbf{u}}{\partial s}\right] \\ = \omega^2\left\{\mathbf{k}\times(\mathbf{k}\times\mathbf{u}) + 2\mathbf{k}\times\frac{\partial \mathbf{u}}{\partial t} + \frac{\partial^2 \mathbf{u}}{\partial t^2} + d_n\mathbf{J}\mathbf{v}_{\mathrm{n}}\right\}\end{aligned} \tag{2.19}$$

and the natural boundary conditions

$$\begin{aligned}&\gamma\left(\frac{\partial \mathbf{r}}{\partial s}.\frac{\partial \mathbf{u}_d}{\partial s}\right)\frac{\partial \mathbf{r}}{\partial s} + p_d\frac{\partial \mathbf{u}_d}{\partial s} \\ &= m\omega^2\left(\mathbf{k}\times(\mathbf{k}\times\mathbf{u}_d) + 2\mathbf{k}\times\frac{\partial \mathbf{u}_d}{\partial t} + \frac{\partial^2 \mathbf{u}_d}{\partial t^2}\right) + d\omega^2\mathbf{J}_d\left(\frac{\partial \mathbf{u}_d}{\partial t} + \mathbf{k}\times\mathbf{u}_d\right).\end{aligned} \tag{2.20}$$

Equations (2.19) and (2.20) can be written in matrix form as

$$\begin{bmatrix}\mathbf{I} & \mathbf{0}\\ \mathbf{0} & \mathbf{I}\end{bmatrix}\begin{Bmatrix}\ddot{\mathbf{u}}\\ \ddot{\mathbf{u}}_d\end{Bmatrix} + \begin{bmatrix}\mathbf{G} & \mathbf{0}\\ \mathbf{0} & \mathbf{G}_d\end{bmatrix}\begin{Bmatrix}\dot{\mathbf{u}}\\ \dot{\mathbf{u}}_d\end{Bmatrix} + \begin{bmatrix}\mathbf{K} & \mathbf{0}\\ \mathbf{0} & \mathbf{K}_d\end{bmatrix}\begin{Bmatrix}\mathbf{u}\\ \mathbf{u}_d\end{Bmatrix} = \mathbf{0}, \tag{2.21}$$

where the Jacobians and the matrix operators are defined in Appendix.

Table 2.1. Non-dimensional parameters

Parameter	Symbol	Range	Type
Angular Velocity	ω	0-3	Variable
Density	ρ	1	Fixed
Elasticity	γ	600	Fixed
End Mass	m	3.5-100	Variable
End Weight	w	3.5-100	Variable
Cable Drag	d_n	0-2000	Variable
Drag Ratio	$f = \frac{d}{d_n}$	0.1-4	Variable
Cable Length	l	1.5-6	Variable

2.4 Non-dimensional Parameter Ranges

The equations of motion include the eight non-dimensional parameters shown in Table 1. The non-dimensional angular velocity is limited by the turning radius and the velocity of the tow vehicle. The non-dimensional angular velocities of the high performance military aircraft used in [2] are about 1.5 while the ship maneuvers in [7] have much smaller angular velocities. Hence, for the analysis angular velocities in the range $0 - 3$ are considered. The non-dimensional cable density ρ is fixed for a given fluid (water or air). Assuming air as the medium, ρ takes the constant value 1 throughout the analysis. Similarly, the elastic parameter γ is held constant at 600 because the steady state solutions and their stability are relatively insensitive to this parameter [8]. The non-dimensional end mass m and weight w have the same numerical values and can therefore be considered as a single design variable ranging from $3.5 - 100$.

The drag coefficients of the cable and end mass are related to the standard coefficients of drag as follows:

$$d = \frac{1}{2}\frac{\rho_{air} A_C C_D}{\rho_a A_0} \tag{2.22}$$

$$d_n = \frac{1}{2}\frac{d_c \rho_{air} C_{Dn} a}{A_0 \rho_a} \tag{2.23}$$

where C_D and C_{Dn} are the standard drag coefficients of the end mass and the cable, respectively, ρ_{air} is the fluid density, d_c is the cable diameter, and A_c is the frontal area of the end mass. A wide range of cross sectional areas for the cable are acceptable design values so the drag coefficients d_n and d can vary by orders of magnitude compared with C_D and C_{Dn} which typically range from $0-1.8$. Therefore, the upper limit in the current analysis is 2000. $d = fd_n$, where f is assumed constant, ranging from $0.1 - 4$. The cable lengths are assumed to lie between 1.5 and 6.

Chapter 3

Design of Single-Valued Steady State Solutions

3.1 Solution Procedure

The steady states solutions of the boundary value problem represented by ODEs (2.11-2.13) with the boundary conditions (2.15-2.17) are solved using the numerical continuation and bifurcation software AUTO [9]. AUTO uses an orthogonal collocation method for solving boundary value problems. An initial guess for the collocation method is generated using a single shooting method, where a value for x_d is assumed at $s = 0$ and the solution of x_d is obtained by minimizing the error $x(l)^2 + y(l)^2 - 1$ at $s = l$ using the optimization routine *fmin* provided by Scipy in the AUTO python interface. Based on this initial approximation the steady state solution curves can be generated using numerical continuation.

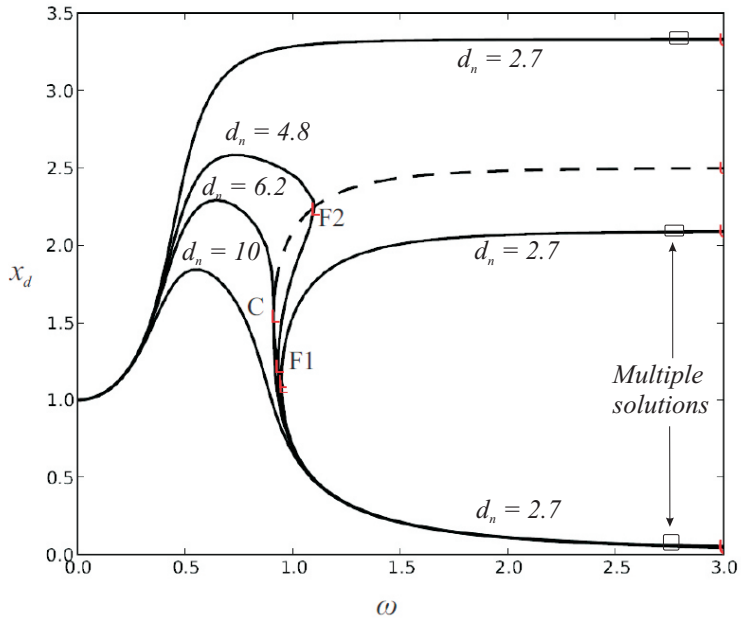

Figure 3.1. Steady state end mass radius x_d versus angular velocity ω for $d_n = 2.7, 4.8, 6.2$ and 10. ($f = 1$, $l = 3$ and $m = 50$). The dashed line shows the continuation path of the turning point F2 as d_n is varied.

3.2 Design

Figure 3.1 shows the steady state end mass radius for different cable drag coefficients in a bifurcation diagram. Cable angular velocity is the continuation parameter in AUTO. The figure shows the existence of multiple solutions, jump phenomena and single valued solutions for different values of the parameters. For low cable drags ($d_n = 2.7$) there are multiple steady state solutions for $\omega > 0.9$. As the drag is increased to 4.8, the multiple isolated solutions become a single continuous curve but multivalued for $0.9 < \omega < 1.1$. In practice, if the angular velocity increases from 0 to 1.1 the radius of the end mass grows slowly and then suddenly jumps from 2.3 to 0.5. For decreasing angular velocity, however, it jumps from 1.3 to 2.5 at the lower angular velocity. If $d_n > 6.2$ then these jump phenomena are no longer observed for $\omega < 3$.

Figure 3.2 plots the turning points or the fold points F1 and F2, corresponding to where

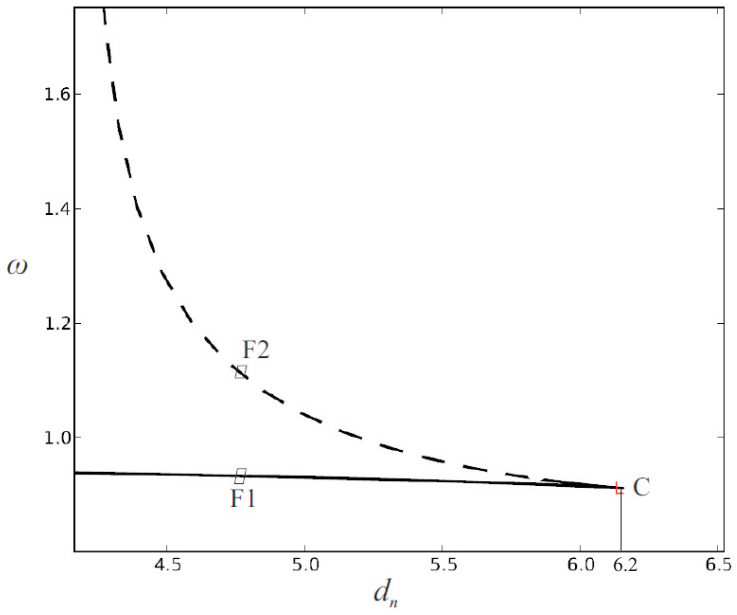

Figure 3.2. Angular velocity at cusp point versus drag coefficient

the slope of the end mass radius x_d with respect to the angular velocity ω becomes infinite. F1 and F2 move closer to each other and finally coalesce into a single cusp point C as the cable drag is increased which defines the minimum damping for single valued solutions.

The locus of the minimum drag coefficients of the cable for the single-valued solutions for different cable lengths and end masses is shown in Fig. 3.3. As the cable length increases the minimum drag required for single valued solutions decreases for a given end mass. With increasing end mass, the required cable drag for single valued solutions increases. Increasing the end mass drag means that less cable drag is required for single valued solutions.

Figure 3.4 plots ω and x_d versus l at the cusp and minimum x_d points for two values of m. The minimum x_d point is a preferable operating point because x_d is small. It is disadvantageous, however, because the required ω is high. The cusp point is not desirable because x_d is high. Increasing m tends to increase w and x_d, decreasing system

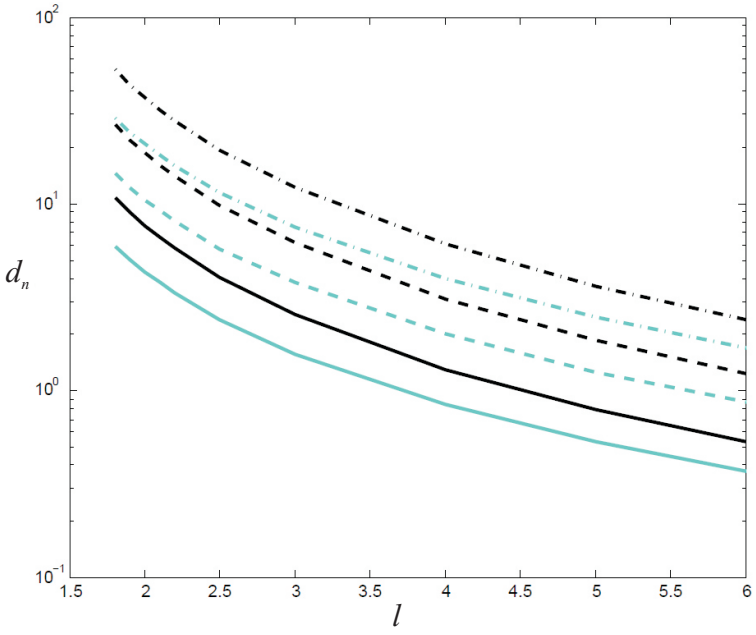

Figure 3.3. Cable drag d_n versus length l boundary for unique solutions with $m = 20$ (solid), $m = 50$ (dashed) and $m = 100$ (dash dotted) and $f = 1$ (dark), $f = 2$ (light)

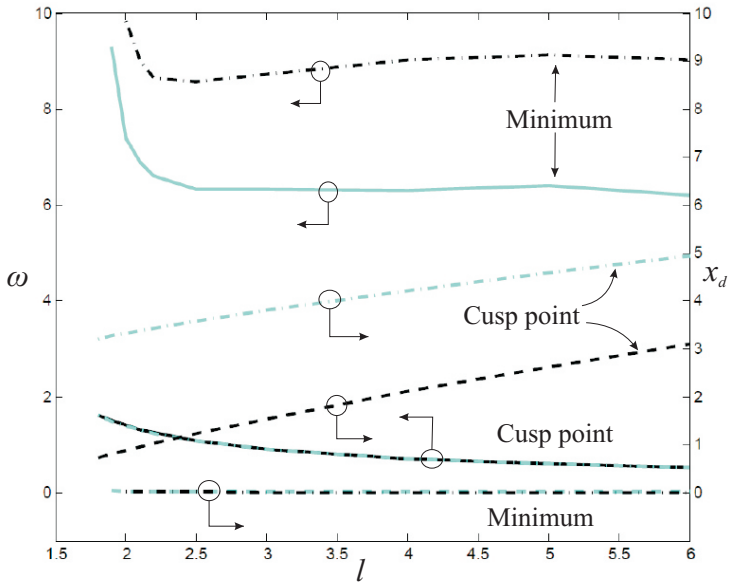

Figure 3.4. Angular velocity ω versus Cable length l at the cusp point (light-solid) and first minimum (dark-solid) and end mass radius x_d versus cable length l at the cusp point (dark-dashed) and first minimum (light-dashed) for $f = 1$ and $m = 50$ and 100 (dash-dotted)

performance.

Chapter 4

Design of Stable Steady State Solutions

4.1 Solution Procedure

The vibration equations from Eq. (2.21) are discretized using Galerkin's method. The displacement is approximated by

$$u_s^p(s,t) = \sum_{j=1}^{N} \eta_{jk}(t)\theta_j(s) \qquad (k = 1, 2, 3), \tag{4.1}$$

where the admissible functions are

$$\theta_j(s) = sin(\beta_j(l-s)/l) \tag{4.2}$$

and β_j are the natural frequencies of a string with one fixed end and other end attached to a mass. Application of Galerkin's method gives the discretized equations

$$\underline{\mathbf{M}}\underline{\ddot{\eta}} + \underline{\mathbf{G}}\underline{\dot{\eta}} + \underline{\mathbf{K}}\underline{\eta} = \underline{\mathbf{0}}, \tag{4.3}$$

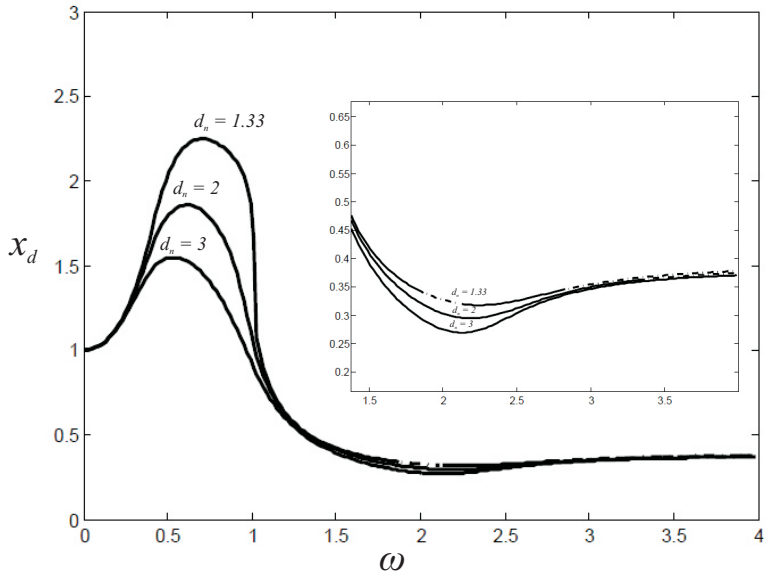

Figure 4.1. Stable(solid) and flutter unstable (dash-dotted) steady state solutions for $d_n = 1.33, 2$, and 3 ($m = 3.5$, $l = 3$ and $f = 0.1$)

where $\underline{\eta} = [\eta_{11}, \eta_{12}, \eta_{13}, \eta_{21}, ..., \eta_{N3}]^T$.

The eigenvalues (λ) of

$$\mathbf{A} = \begin{bmatrix} \underline{\mathbf{0}} & \underline{\mathbf{I}} \\ -\underline{\mathbf{M}}^{-1}\underline{\mathbf{K}} & -\underline{\mathbf{M}}^{-1}\underline{\mathbf{G}} \end{bmatrix}$$

define stability. If the real parts of all the eigenvalues are negative the system is stable.

4.2 Design

Figure 4.1 shows the stable (solid) and flutter unstable (dash-dotted) steady state solutions for three different drag coefficients. The inset shows an enlarged version of the stability curves for higher angular velocities. For the $d_n = 1.33$ the solutions are unstable for $2.8 < \omega < 4.0$ and $1.8 < \omega < 2.2$. At $d_n = 2.0$ the unstable region is reduced to $3.2 < \omega < 4$ and the solutions are completely stable for $d_n = 3$. In general, the sta-

ble regions increase with increasing cable drag. There is a minimum cable drag above which the solution is stable for $\omega < 3$. There is also a minimum for the radius of the end mass near $\omega = 2.1$. The angular velocity corresponding to this first minimum of the radius of the end mass is a favorable design point. The minimum drag coefficient of the cable for which the steady state solution is stable at this minimum defines the desired design condition for the CTCBS with stable steady state solutions with low end mass radius.

The locus of minimum d_n required for stable steady state solutions is shown in Fig 4.2. As with minimum drag for single valued solutions, the minimum d_n that ensures stable solutions also decreases with the increasing cable length and decreasing end mass. To achieve the overall objective of single valued and stable solutions, the maximum of the minimum values from Figs. 3.3 and 4.2 should be used.

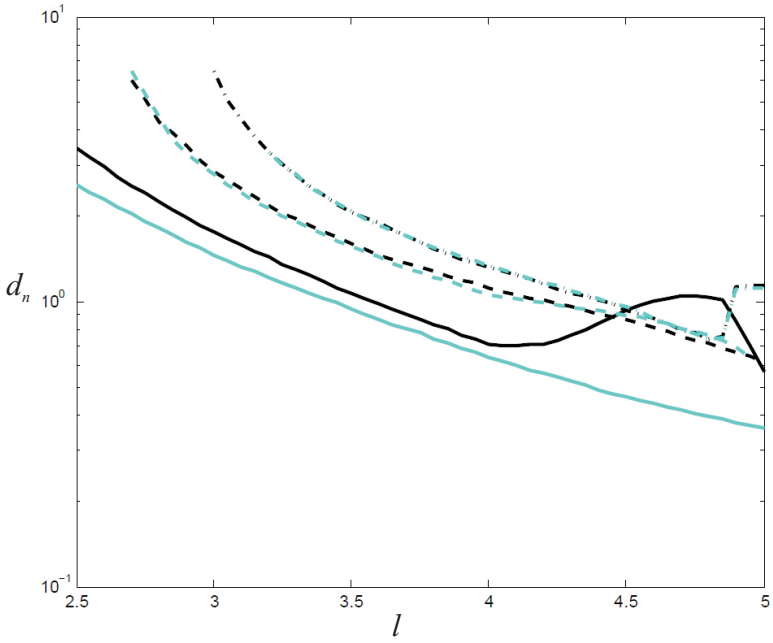

Figure 4.2. Cable drag d_n versus length l boundary for stable solutions with $m = 20$ (solid), $m = 50$ (dashed) and $m = 100$ (dash-dotted) and $f = 1$ (dark) and and $f = 2$ (light)

Chapter 5

Design Example

The design of CTCBS is performed in dimensional space based on the results from the previous sections as outlined in the flowchart in Fig. 5.1. Consider as an example an aircraft acting as a tow vehicle moving at a constant speed of 50 m/s. The minimum turning radius of the aircraft is assumed to be 100 m, yielding $\omega = 1.6$. In practice, the circular motion of the aircraft is only approximate and the aircraft orbit varies about a mean value. Assuming that $a = 100 - 250$ m, the corresponding $\omega = 1.0 - 1.6$. A cable with $L = 500$ m gives a non-dimensional length $l = 2 - 5$. The payload for the application is assumed to be $M = 1$ kg. Further, the cable is assumed to have a density of 1100 kg/m^3 and a diameter of $D = 0.48$ mm. Then, the $m = 20 - 50$. If the cable and the end mass have drag coefficients $C_{Dn} = 0.6$, $C_D = 1.6$, respectively, then the associated $d_n = 85.36 - 213.41$ and $d = 9.3$, respectively. From Fig. 3.4, $\omega = 1.6$ for a cable with $l = 5$ is acceptable for the design. For the lower cable length ($l = 2$), however, the angular velocity ($\omega = 1.0$) falls short of the cusp point and the cable length should be increased. A cable length $L = 1000$ m gives $l = 4$ which makes $\omega = 1.0$ which is greater than the angular velocity at the cusp point and is hence acceptable for the design. The drag coefficient ratio $f = 0.1$ and 0.04 for $a = 100$ and

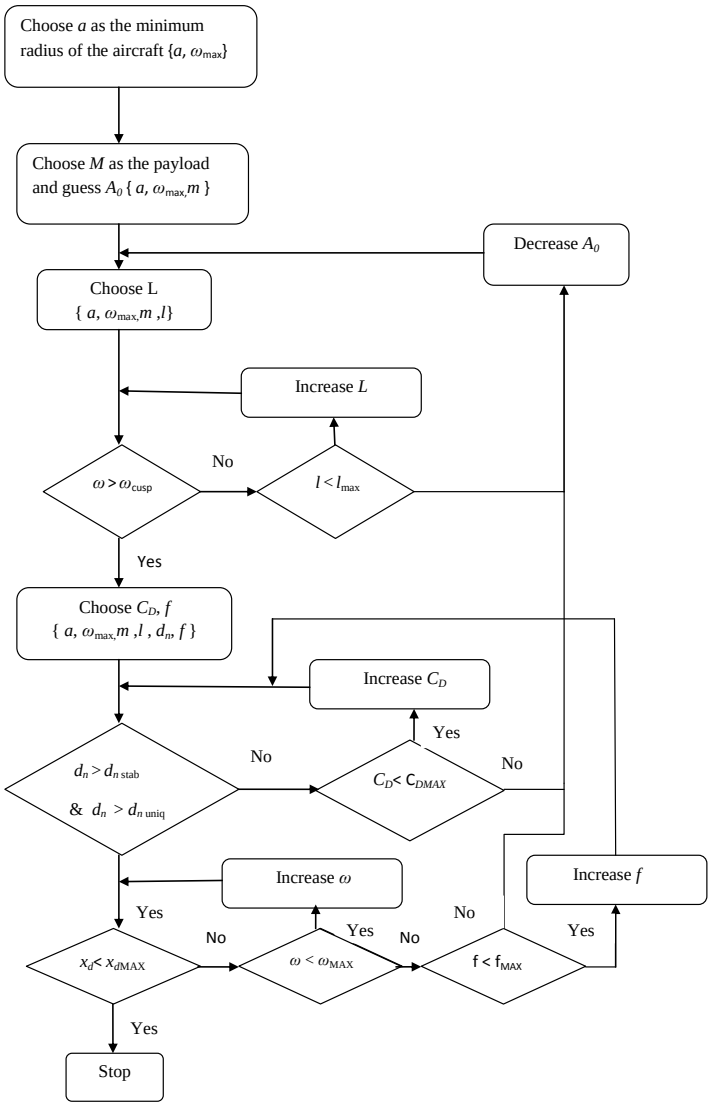

Figure 5.1. Flowchart showing the procedure for the design

250, respectively. The drag coefficients for the given mass and cable length are higher than the required cable drags in Fig. 3.3 and 4.2 even if the lower f were to shift the curves slightly upwards. In general, if the cross sectional area is sufficiently low, then the non-dimensional drag coefficients are higher than the design requirements.

The radius of the end mass remains to be minimized. The radius $x_d = 0.15$ and 8.43×10^{-3} at $\omega = 1.0$ and 1.6, respectively. While the latter is close to zero, the former can

be further reduced by increasing the cable drag. The material is assumed fixed, so the drag coefficient cannot be varied much but the area of cross section of the cable can be reduced to increase the non-dimensional drag coefficients. Decreasing the area of cross section also increases the non-dimensional mass. This results in a small decrease in the radius of the end mass giving almost the same radius 0.14 for half the cable diameter. This problem can be circumvented by increasing the the drag on the end mass. Increase of $f = 0.04$ to $f = 0.1$ reduces the radius of the end mass from 0.15 to 0.08. In general, the radius of the end mass can be reduced by increasing the fraction f while the other parameters fixed. This can be achieved by changing the geometry and the roughness of the end mass to increase the drag coefficient by increasing the area or using drag chutes on the end mass.

Table 5.1 summarizes the system parameters for the optimal design. Figure 5.2 shows the radius x_d of the end mass as a function of the radius of the tow vehicle a. In this figure, the steady state solutions are stable for all values of a. For lower radius Figure 5.3 shows the same radius of the end mass x_d as a function of cable length l as it varies from 0 to 4 during deployment operation. The steady state solutions are stable for all values of cable lengths l.

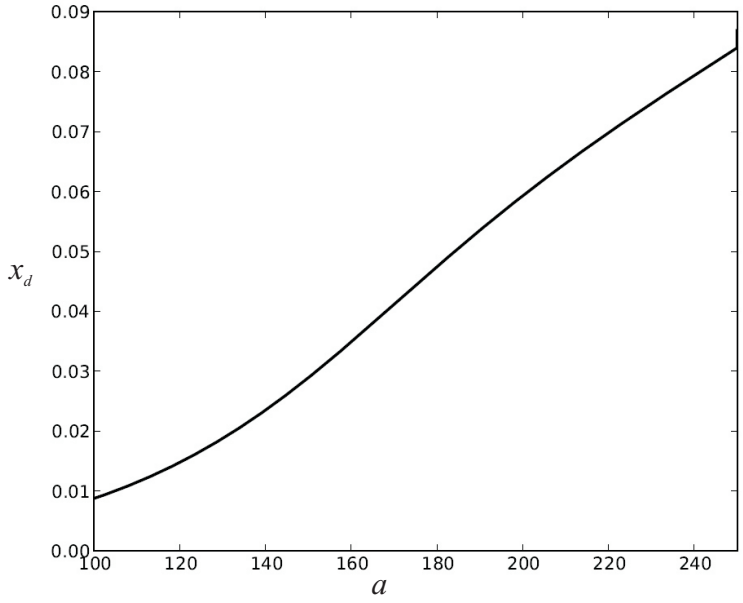

Figure 5.2. Radius of end mass x_d versus radius of the tow vehicle a(m) for the design example. All solutions are stable.

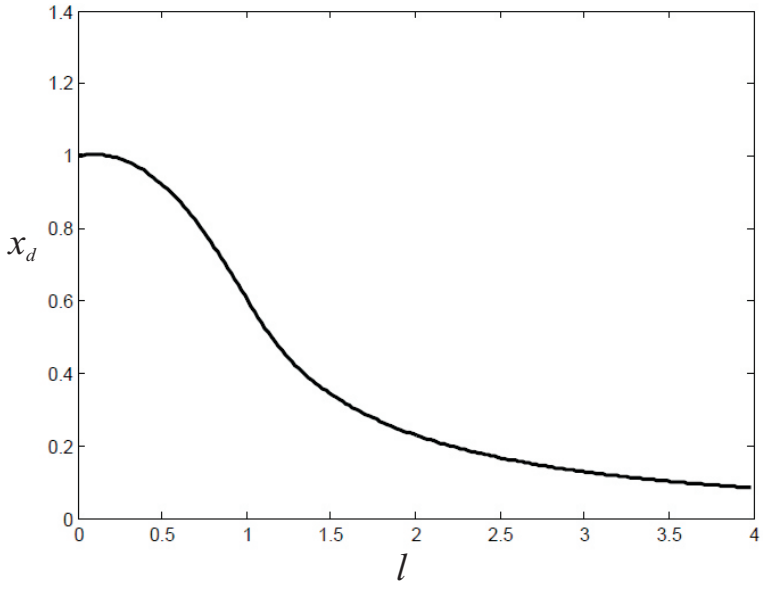

Figure 5.3. Radius of the end mass x_d as a function of deployment length l. All solutions are stable.

Table 5.1. Summary of the design of circularly towed cable body system

Parameter	**Symbol**	**Value**
Aircraft Speed	V	50m/s
Turning Radius	a	100-250m
Cable Length	L	1000m
Payload	M	1Kg
Drag Coefficient of the cable	C_{Dn}	0.6
Drag Coefficient of the End Mass	C_D	1.6
Density of the Cable	ρ_a	1100Kg/m^3
Diameter of the Cable	d_c	0.00048m
Frontal area of the end mass	A_C	0.045 m^2
Young's Modulus	E	2GPa

Chapter 6

Conclusions

The design of the CTCBS requires that the steady state solutions are stable and single valued and have low end mass radius throughout the operating region. In general, stability increases with increasing damping, decreasing end mass, and increasing cable length. In practice, other than placing a drag chute on the end mass, it is very difficult to modify damping. The cable diameter and material are often specified by cost, availability, and strength. The end mass is also dictated by the application but this analysis indicates that it should be as small as possible. Cable length varies during deployment so it may be advisable to deploy the cable prior to initiating a transition to circular orbit. As the drag coefficient of the cable increases, steady state solutions that exhibit multiple solutions become single valued solutions and instability regions disappear. The maximum of the minimum d_n required for the uniqueness and stability of the steady state solutions defines the minimum d_n required for the design. The end mass radius is close to the radius of the tow vehicle for the angular velocities below the cusp point and has a minimum at higher rotational rates.

Appendix A

A.1 Jacobian Matrix

In equation (2.6), $\mathbf{v}_n^f$ can be expressed as

$$\mathbf{v}_n^f = \mathbf{v}_n^i + \mathbf{v}_n \tag{A.1}$$

where $\mathbf{v}_n^i$ is obtained by substitutiong $\mathbf{u} = 0$ in equation (2.6) and equation (A.1) defines $\mathbf{v}_n$

Linearization of air drag force produces

$$d_n|\mathbf{v}_n^f|\mathbf{v}_n^f = d_n(|\mathbf{v}_n^i|\mathbf{v}_n^i + \mathbf{J}\mathbf{v}_n)$$

where the Jacobian Matrix is

$$\mathbf{J} = \frac{\partial(|\mathbf{v}_n^f|\mathbf{v}_n^f)}{\partial \mathbf{v}_n^f}\bigg|_{\mathbf{v}_n=0} = \begin{bmatrix} J_1 & J_2 & J_3 \\ J_2 & J_4 & J_5 \\ J_3 & J_5 & J_6 \end{bmatrix} = |\mathbf{v}_n^i|\mathbf{I} + \frac{1}{|\mathbf{v}_n^i|}\begin{bmatrix} x_1^2 & x_1x_2 & x_1x_3 \\ x_1x_2 & x_2^2 & x_2x_3 \\ x_xx_3 & x_2x_3 & x_3^2 \end{bmatrix}$$

and

$$x_1 = -y + x_{,s}(yx_{,s} - y_{,s}x), x_2 = x + y_{,s}(xy_{,s} - x_{,s}y), x_3 = z_{,s}(yx_{,s} - xy_{,s})$$
$$|\mathbf{v}_n^i| = \sqrt{x_1^2 + x_2^2 + x_3^2}$$

and $\mathbf{I}$ is the unit matrix. To calculate $\mathbf{J}_d$, one has

$$\mathbf{v}_d^f = \mathbf{v}_d^i + \mathbf{v}_d$$

where $\mathbf{v}_d^i = \mathbf{k} \times \mathbf{r}$ and $\mathbf{v}_d = \frac{\partial \mathbf{u}}{\partial t} + \mathbf{k} \times \mathbf{u}$ Hence,

$$\mathbf{J}_d = \left. \frac{\partial(|\mathbf{v}_d^f|\mathbf{v}_d^f)}{\partial \mathbf{v}_d^f} \right|_{\mathbf{v}_d=0} = \sqrt{y^2+x^2}\mathbf{I} + \frac{1}{\sqrt{y^2+x^2}} \begin{bmatrix} y^2 & -xy & 0 \\ -xy & x^2 & 0 \\ 0 & 0 & 0 \end{bmatrix}$$

At $s = 0$, $y = 0$ and $x = x_d$, one has

$$\mathbf{J}_d = \begin{bmatrix} x_d & 0 & 0 \\ 0 & 2x_d & 0 \\ 0 & 0 & x_d \end{bmatrix}$$

Appendix B

B.1 Matrix Operators

In equation (2.23), $\mathbf{G}$ is defined as

$$\mathbf{G} = \mathbf{G}_0 + d_n\mathbf{D}$$

where

$$\mathbf{G}_0 = \begin{bmatrix} 0 & -2 & 0 \\ 2 & 0 & 0 \\ 0 & 0 & 0 \end{bmatrix}$$

$$\begin{aligned}
\mathbf{D}(1,1) &= -J_2x_{,s}y_{,s} + J_1y_{,s}^2 + J_1z_{,s}^2 - J_3x_{,s}z_{,s} \\
\mathbf{D}(1,2) &= -J_3y_{,s}z_{,s} + J_2z_{,s}^2 + J_2x_{,s}^2 - J_1y_{,s}x_{,s} \\
\mathbf{D}(1,3) &= -J_2z_{,s}y_{,s} + J_3y_{,s}^2 + J_3x_{,s}^2 - J_1x_{,s}z_{,s} \\
\mathbf{D}(2,1) &= -J_4x_{,s}y_{,s} + J_2z_{,s}^2 + J_2y_{,s}^2 - J_5x_{,s}z_{,s} \\
\mathbf{D}(2,2) &= -J_5y_{,s}z_{,s} + J_4x_{,s}^2 + J_4z_{,s}^2 - J_2x_{,s}y_{,s} \\
\mathbf{D}(2,3) &= -J_4y_{,s}z_{,s} + J_5y_{,s}^2 + J_5x_{,s}^2 - J_2x_{,s}z_{,s} \\
\mathbf{D}(3,1) &= -J_5x_{,s}y_{,s} + J_3y_{,s}^2 + J_3z_{,s}^2 - J_6x_{,s}z_{,s} \\
\mathbf{D}(3,2) &= -J_6y_{,s}z_{,s} + J_5x_{,s}^2 + J_5z_{,s}^2 - J_3y_{,s}x_{,s} \\
\mathbf{D}(3,3) &= -J_3x_{,s}z_{,s} + J_6y_{,s}^2 + J_6x_{,s}^2 - J_5y_{,s}z_{,s}
\end{aligned}$$

The matrix operator $\mathbf{K}$ is

$$\mathbf{K} = \mathbf{K}_0 + (\mathbf{K}_s + d_n\mathbf{K}_{s0})\frac{\partial}{\partial s} + \mathbf{K}_{ss}\frac{\partial^2}{\partial s \partial s}$$

where

$$\begin{aligned}
\mathbf{K}_0(1,1) &= -1 + d_n(J_2 x_{,s}^2 + J_2 z_{,s}^2 - J_3 y_{,s} z_{,s} - J_1 y_{,s} x_{,s}) \\
\mathbf{K}_0(1,2) &= d_n(-J_1 y_{,s}^2 - J_1 z_{,s}^2 + J_2 y_{,s} x_{,s} + J_3 z_{,s} x_{,s}) \\
\mathbf{K}_0(2,1) &= d_n(J_4 z_{,s}^2 + J_4 x_{,s}^2 - J_2 y_{,s} x_{,s} - J_5 z_{,s} y_{,s}) \\
\mathbf{K}_0(2,2) &= -1 + d_n(J_5 x_{,s} z_{,s} - J_2 y_{,s}^2 - J_2 z_{,s}^2 + J_4 y_{,s} x_{,s}) \\
\mathbf{K}_0(3,1) &= d_n(J_5 x_{,s}^2 + J_5 z_{,s}^2 - J_6 y_{,s} z_{,s} - J_3 x_{,s} y_{,s}) \\
\mathbf{K}_0(3,2) &= d_n(-J_3 z_{,s}^2 - J_3 y_{,s}^2 + J_6 z_{,s} x_{,s} + J_5 x_{,s} y_{,s}) \\
\mathbf{K}_0(1,3) &= 0, \quad \mathbf{K}_0(2,3) = 0, \quad \mathbf{K}_0(3,3) = 0,
\end{aligned}$$

$$\mathbf{K}_s = \frac{1}{\omega^2}\begin{bmatrix} -p_{,s} - 2\gamma x_{,s} x_{,ss} & -\gamma(x_{,s} y_{,ss} + x_{,ss} y_{,s}) & -\gamma(x_{,s} z_{,ss} + x_{,ss} z_{,s}) \\ -\gamma(x_{,s} y_{,ss} + x_{,ss} y_{,s}) & -p_{,s} - 2\gamma y_{,s} y_{,ss} & -\gamma(y_{,s} z_{,ss} + y_{,ss} z_{,s}) \\ -\gamma(x_{,s} z_{,ss} + x_{,ss} z_{,s}) & -\gamma(y_{,s} z_{,ss} + y_{,ss} z_{,s}) & -p_{,s} - 2\gamma z_{,s} z_{,ss} \end{bmatrix}$$

$$\begin{aligned}
\mathbf{K}_{s0}(1,1) &= 2J_2 x x_{,s} + J_3 y z_{,s} - J_1 y_{,s} x + J_2 y y_{,s} \\
\mathbf{K}_{s0}(1,2) &= -2J_1 y y_{,s} - J_1 x x_{,s} + J_2 x_{,s} y - J_3 x z_{,s} \\
\mathbf{K}_{s0}(1,3) &= J_3 y x_{,s} - 2J_1 y z_{,s} - J_3 y_{,s} x + 2J_2 x z_{,s} \\
\mathbf{K}_{s0}(2,1) &= -J_2 y_{,s} x + J_4 y y_{,s} + 2J_4 x x_{,s} + J_5 y z_{,s} \\
\mathbf{K}_{s0}(2,2) &= -J_2 x x_{,s} + J_4 y x_{,s} - J_5 z_{,s} x - 2J_2 y y_{,s} \\
\mathbf{K}_{s0}(2,3) &= 2J_4 x z_{,s} - J_5 x y_{,s} + J_5 y x_{,s} - 2J_2 z_{,s} y \\
\mathbf{K}_{s0}(3,1) &= -J_3 x y_{,s} + J_5 y y_{,s} + 2J_5 x_{,s} x + J_6 y z_{,s} \\
\mathbf{K}_{s0}(3,2) &= -J_3 x x_{,s} - J_6 x z_{,s} - 2J_3 y_{,s} y + J_5 y x_{,s} \\
\mathbf{K}_{s0}(3,3) &= 2J_3 y z_{,s} + 2J_5 x z_{,s} - 2J_6 y_{,s} x + J_6 x y_{,s}
\end{aligned}$$

$$\mathbf{K}_{ss} = \frac{1}{\omega^2} \begin{bmatrix} -\gamma x_{,s}^2 - p & -\gamma x_{,s} y_{,s} & -\gamma x_{,s} z_{,s} \\ -\gamma x_{,s} y_{,s} & -\gamma y_{,s}^2 - p & -\gamma y_{,s} z_{,s} \\ -\gamma x_{,s} z_{,s} & -\gamma y_{,s} z_{,s} & -\gamma z_{,s}^2 - p \end{bmatrix}$$

Finally, $\mathbf{G}_d$ and $\mathbf{K}_d$ are given by

$$\mathbf{G}_d = \frac{1}{m} \begin{bmatrix} dx_d & -2m & 0 \\ 2m & 2dx_d & 0 \\ 0 & 0 & dx_d \end{bmatrix}$$

$$\mathbf{K}_d = \mathbf{K}_{d0} + \mathbf{K}_{ds} \frac{\partial}{\partial s}$$

where

$$\mathbf{K}_{d0} = \frac{1}{m} \begin{bmatrix} -m & -dx_d & 0 \\ 2dx_d & -m & 0 \\ 0 & 0 & 0 \end{bmatrix}$$

$$\mathbf{K}_{ds} = \frac{1}{m\omega^2} \begin{bmatrix} -\gamma x_{,s}^2 - p & -\gamma x_{,s} y_{,s} & -\gamma x_{,s} z_{,s} \\ -\gamma x_{,s} y_{,s} & -\gamma y_{,s}^2 - p & -\gamma y_{,s} z_{,s} \\ -\gamma x_{,s} z_{,s} & -\gamma y_{,s} z_{,s} & -\gamma z_{,s}^2 - p \end{bmatrix} \Bigg|_{s=0}$$

Appendix C

C.1 Admissible Functions

Consider the constant tension cable equation

$$p_d u_{,ss} = u_{,tt} \tag{C.1}$$

subjected to the boundary conditions

$$u(l,t) = 0 \qquad and \qquad p_d u_{,s}(0,t) = m u_{,tt}(0,t) \tag{C.2}$$

The assumed solution

$$u = sin\left(\beta \frac{l-s}{l} e^{i\alpha t}\right) \tag{C.3}$$

yields a frequency equation

$$cos\beta = m\frac{\beta}{l} sin\beta \tag{C.4}$$

with an infinite number of solutions β_i. The admissible functions used are

$$\theta_j(s) = sin\left(\beta_j \frac{l-s}{l}\right) \tag{C.5}$$

Appendix D

D.1 Sensitivity of elastic parameter and drag coefficient of the cable

The steady state solutions and their stability are relatively insensitive [1] to the elastic parameter except for high rotational frequencies and large radius of the end mass. Hence, the elastic parameter γ is assumed to be constant throughout the analysis. The drag coefficient of the end mass is assumed to be a constant fraction f of the cable drag

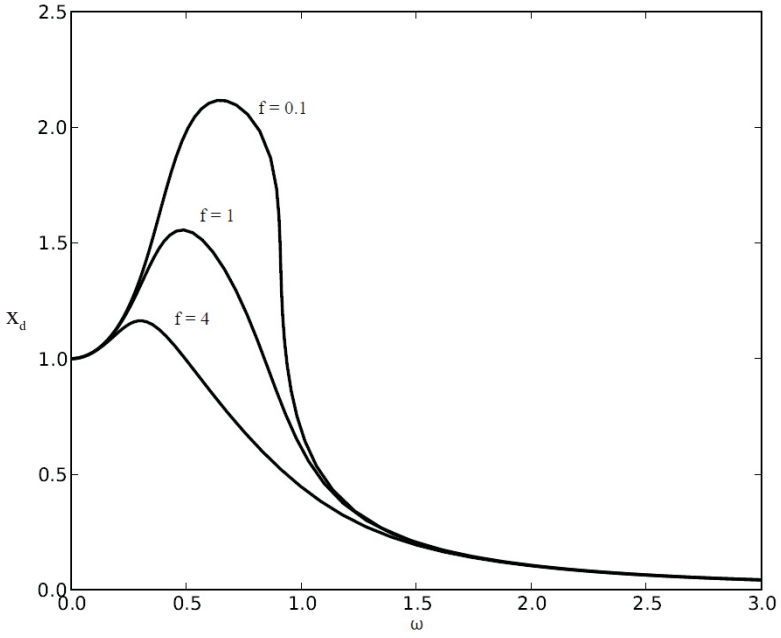

Figure D.1. Sensitivity of the radius of the end mass x_d to the ratio f

for the previous analysis. In Figs. 3.3 and 4.2, the dark curves represent the minimum drag coefficient of the cable for the ratio $f = 1$ and the light curves represent the ratio $f = 2$. In general, The minimum cable drag required reduces as f is increased for both uniqueness and stability curves. The nature of the solutions, however, did not change by changing f. Figure D.1 shows the radius of the end mass for $\omega < 3$ for different values of f. As the ratio f is increased, the radius of the end mass decreased for the lower angular velocities and is a choice for designing for low end mass radius.

Bibliography

[1] RUSSEL, J. J. and W. J. ANDERSON "Equilibrium and stability of a circularly towed cable subject to aerodynamic drag," *ASME, and SAE, Structures, Structural Dynamics, and Materials Conference*, **1**(5), pp. 80–88.

[2] WILLIAMS, P. and P. TRIVALIO "Dynamics of Circularly Towed Cable Systems Part 1: Optimal Configurations and Their Stability," *Journal of Guidance, Control, and Dynamics*, **30**(3), pp. 753–765.

[3] CHOO, Y. (1970) *Analytical investigation of the three-dimensional motion of towed systems*, PhD Thesis, The Catholic University of America.

[4] MACARTHUR, D. K., E. Z. MACARTHUR, C. D. CRANE, W. DIXON, V. GOTTIMUKKALA, and C. RAHN (2010) "Autonomous aerial recovery of unmanned aircraft," in *Proceedings Unmanned Systems North America*, Aerial Unmanned Systems International.

[5] ZHU, F. and C. RAHN "Stability analysis of a circularly towed cable-body system," *Journal of Sound and Vibrations*, **217**(3), pp. 435–452.

[6] CLARK, J. D., W. B. FRASER, C. D. RAHN, and A. RAJMANI "Limit-cycle oscillations of a heavy whirling cable subject to aerodynamics drag," *Proceedings of the Royal Society A*, **461**(2055), pp. 875–893.

[7] GROSENBAUGH, M. A. "Transient behavior of towed cable systems during ship turning maneuvers," *Ocean Engineering*, **34**(11), pp. 1532–1542.

[8] ZHU, F., R. SHARMA, and C. RAHN (1997) "Vibrations of elastic ballooning strings," *ASME Journal of Applied Mechanics*, **64**(3), pp. 676–683.

[9] DOEDEL, E. J. and B. E. OLDEMAN (2007), "AUTO-07p: Continuation and bifurcation software for ordinary differential equations," .